RSC Advances

PAPER

View Article Online
View Journal | View Issue

Cite this: *RSC Adv.*, 2021, **11**, 17437

Ultra-stretchable and healable hydrogel-based triboelectric nanogenerators for energy harvesting and self-powered sensing†

Guoxia Li,[ab] Longwei Li,[bc] Panpan Zhang,*[b] Caiyun Chang,[ab] Fan Xu[bc] and Xiong Pu *[abc]

Received 13th March 2021
Accepted 19th April 2021

DOI: 10.1039/d1ra02010b

rsc.li/rsc-advances

The next-generation multifunctional soft electronic devices require the development of energy devices possessing comparable functions. In this work, an ultra-stretchable and healable hydrogel-based triboelectric nanogenerator (TENG) is prepared for mechanical energy harvesting and self-powered sensing. An ionic conductive hydrogel was developed with graphene oxide and Laponite. as the physical cross-linking points, exhibiting high stretchability (~1356%) and healable capability. When using the hydrogel as the electrode, the TENG can operate normally at 900% tensile strain, while the electrical output of the TENG can fully recover to the initial value after healing the damage. This hydrogel-based TENG is demonstrated to power wearable electronics, and is used as a self-powered sensor for human motion monitoring and pressure sensing. Our work shows opportunities for multifunctional power sources and potential applications in wearable electronics.

1. Introduction

Wearable electronic devices have attracted intense attention in the last decade with multiple functions being realized, such as transparency, stretchability, biocompatibility, healable capability, and biodegradability.[1–6] A variety of electronic devices have been designed and developed, but most of them are powered by traditional power sources, such as heavy batteries and capacitors which have limited life span and are not environmentally friendly. It is still a bottleneck challenge to provide sustainable power to these electronic devices without sacrificing their advantages in stretchability or other functions. Therefore, it has become an alternative technology approach to develop energy harvesters with compatible multifunctions, so as to scavenge the distributed renewable energies in the working environment of these devices for the power sources.

Triboelectric nanogenerators (TENGs) have intensively been studied in recent for energy harvesting and self-powered sensors.[7–11] The TENG generates electricity from various kinetic energies based on the effects of triboelectric electrification and electrostatic induction. It has the advantages of low cost, high flexibility, high efficiency, and environmental friendliness. Efforts have been also made to develop multifunctional TENGs, such as stretchable, transparent, healable, or biodegradable TENGs.[12–21] The key to achieve stretchable TENGs is the development of stretchable electrodes. Stretchable TENGs have been reported using electrodes of conductive filler-percolated composites,[22–24] liquid metals,[25–28] ionic solutions,[29] or ionic gels.[30,31] The ion-conducting gel electrodes, including hydrogels, ionogels and organogels, have the advantages of low modulus and high stretchability. Even though their conductivity is generally much lower than that of electronic conductors, it overcomes the low stretchability of electronic conductors, since the ion conduction is based on the ion transfers along the trapped solution inside the molecular networks.[32] Furthermore, it is easier for gel electrodes to achieve other multifunctions through the design of proper molecular chain networks, such as the healable capability, biodegradability or transparency. In particular, the hydrogels have the highest conductivity and are more environmentally friendly or biocompatible than the other two counterparts. Therefore, efforts are still being made to optimize the hydrogel electrode-based multifunctional TENGs.

Here, we present an ultra-stretchable and healable hydrogel-based TENG for mechanical energy harvesting. Graphene oxide (GO) and Laponite were used as collaborative physical cross-linking points in the hydrogel, leading to its high stretchability and high healable efficiency. The hydrogel with 1 wt% GO achieved a tensile strength of 106 kPa and an ultimate tensile strain of 1356%, and the ionic conductivity is 38.8 mS cm^{-1} at

[a]*School of Chemistry and Chemical Engineering, Center on Nanoenergy Researh, School of Physical Science and Technology, Guangxi University, Nanning 530004, China*

[b]*CAS Center for Excellence in Nanoscience, Beijing Key Laboratory of Micro-Nano Energy and Sensor, Beijing Institute of Nanoenergy and Nanosystems, Chinese Academy of Sciences, Beijing 101400, China. E-mail: puxiong@binn.cas.cn; zhangpanpan@binn.cas.cn*

[c]*School of Nanoscience and Technology, University of Chinese Academy of Sciences, Beijing 100049, China*

† Electronic supplementary information (ESI) available. See DOI: 10.1039/d1ra02010b

25 °C. All the aforementioned characteristics make this hydrogel useful as an electrode for stretchable and healable TENG. The obtained TENG can not only maintain high stretchability, but can also fully recover its electricity generation capability after healing the damages autonomously. Moreover, these TENG could also function as sensors for detecting human motions and contacting pressures.

2. Experimental

2.1 Preparation of Laponite/poly(AMPS-*co*-AA-*co*-DMAPMA)/GO–LiCl (LPG–LiCl) hydrogels

Laponite/poly(AMPS-*co*-AA-*co*-DMAPMA)/GO–LiCl hydrogels is wrote as LPG–LiCl hydrogels for short. The hydrogel was prepared according to the previously reported method.[33,34] The GO and Laponite were acted as collaborative cross-linking points. The Laponite used was a kind of laminated clay with a thickness of about 1 nm and a diameter of about 30 nm ($Mg_{5.34}Li_{0.66}Si_8O_{20}(OH)_4Na_{0.66}$, NANOCOR Co., U.S.). Typically, GO (1 wt% relative to monomer) was dispersed in 8 mL deionized water with continuous stirring for 20 min to achieve homogeneous dispersion, followed by ultrasonic vibration for 30 min, and then 0.2474 g of Laponite was added into the GO suspension with stirring for 20 min and ultrasonically dispersed for about 30 min. A desired amount of sodium pyrophosphate was added into the dispersion to reduce the viscosity. The mass ratio of sodium pyrophosphate to Laponite was kept at 0.0768 : 1. Then AMPS was added and stirred for another 20 min. Afterward, 6.0 mL of AA was neutralized to a neutralization degree of 40 mol% with 30 wt% NaOH solution in an ice bath. Subsequently, DMAPMA, LiCl (2 M relative to deionized water), initiator KPS, and catalyst TEMED were added to the system under stirring. In all cases, the molar ratio of total monomers to KPS to TEMED was kept at 100 : 0.37 : 0.638. Finally, the polymerization was performed in a glass tube at 50 °C for 72 h.

2.2 Fabrication of the TENG

The VHB film (3 M VHB 9469, thickness is 130 μm) was used as electrification layer, the LPG–LiCl hydrogel was cut into the desired shape with a sharp scissor. The final device was fabricated by wrapping and sealing the hydrogel with the VHB films. A Cu wire was attached to the hydrogel for electrical connection.

2.3 Characterization and measurements

The electrochemical performance was measured by CHI 760E electrochemical workstation. The resistance of hydrogel was measured by an Interactive digital instrument (2450 SourceMeter, Keithley). Fourier transform infrared (FTIR) analysis spectra of Laponite, GO, and dry hydrogels were conducted through an IR spectrophotometer (Frontier FT-IR) with the range of wavenumbers from 400 to 4000 cm^{-1}. The scanning electron microscopy (SEM) images of samples were obtained using SU 8010 at an accelerating voltage of 5 kV. The mechanical tensile test and stretch cycling test of the hydrogels were conducted by an ESM301/Mark-10 system. For the tensile test and the cyclic tensile test, the strain rate was fixed at 50 mm min^{-1}. Use the optical microscope Axio Imager.M2m to observe the healable behavior of the hydrogel. A step motor (LinMot E1100) was used to provide the input of mechanical motions. The voltage, current and charge quantity were recorded by a Keithley electrometer 6517.

3. Results and discussions

3.1 Fabrication and characterization of the hydrogel

The hydrogel polymer chains are prepared by co-polymerization of three monomers, *i.e.* 2-acrylamido-2-methylpropane sulfonic acid (AMPS), acrylic acid (AA) and *N*-[3-(dimethylamino)propyl] methacrylamide (DMAPMA), as shown in Fig. 1a. The GO and Laponite were added as physical crosslinking points (Fig. 1b). Laponite and GO, which both have similar laminated

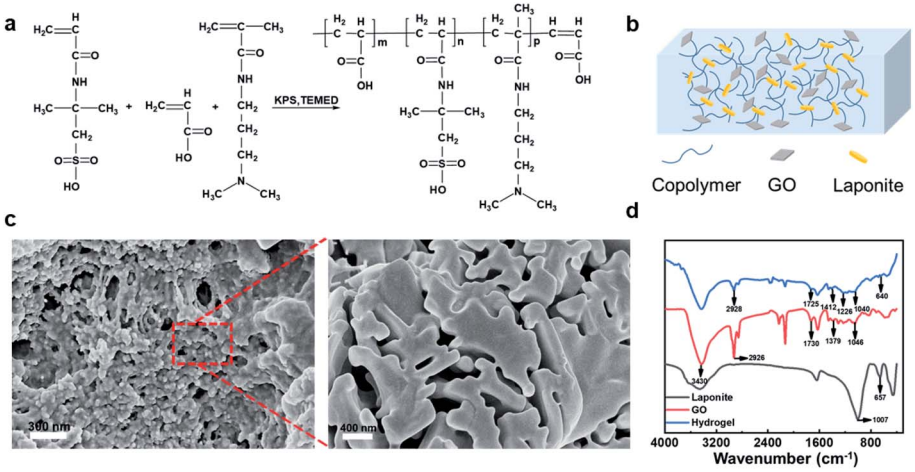

Fig. 1 Preparation of the nanocomposite LPG–LiCl hydrogels. (a) Schematic of copolymerization of poly(AMPS-*co*-AA-*co*-DMAPMA) with potassium persulfate (KPS) and *N*,*N*,*N*′,*N*′-tetramethylethylenediamine (TEMED) as initiator and catalyst, respectively. (b) Schematic network structure of LPG–LiCl hydrogels with Laponite and GO as cross-linking points. (c) SEM images of a freeze-dried LPG–LiCl hydrogel. (d) FTIR spectra of Laponite, GO, and LPG–LiCl hydrogels.

structures, can enhance the mechanical properties of hydrogels, achieving high strength and high stretchability.[35,36] Meantime, they can endow the systems healable property due to the formation of abundant hydrogen bondings. The Laponite–GO-crosslinked poly(AMPS-*co*-AA-*co*-DMAPMA) hydrogels with 2 M LiCl was noted as LPG–LiCl hydrogel thereafter. The scanning electron microscopy (SEM) images of the freeze-dried hydrogel samples showed that the polymer matrix had a typical three-dimensional porous morphology, which is beneficial for the uptake of aqueous solution (Fig. 1c). From the FTIR spectra (Fig. 1d), the reflection peak of stretching vibrations of Si–O–Si in Laponite at 657 cm^{-1} shifted to a lower wavenumber of 640 cm^{-1} in the hydrogel, indicating that crosslinking by hydrogen bonds was formed between Laponite and polymer chains. As for the GO, reflection peak at 3430 cm^{-1} was attributed to the O–H stretching; reflection peaks at 1730 cm^{-1} and 1379 cm^{-1} were attributed to the C=O and C–OH in the COOH groups, respectively; reflection peak at 1046 cm^{-1} and C–O–C stretching vibrations. However, the C=O peak of GO in the hydrogel shifted to a lower wavenumber of 1725 cm^{-1}, indicating the existence of hydrogen bonds between GO and polymer chains.

Fig. 2a showed the variation of the tensile strength and strain at break of the LPG hydrogel with different GO contents. The tensile strength and strain at break for the hydrogel without GO is 43 kPa and 2948%, respectively. When the GO content was 1 wt%, the tensile strength was 106 kPa, more than 2 times higher than that without GO, but the strain decrease to 1356%. When the content of GO was further increased, the tensile strength of the hydrogel would decrease. Therefore, adding appropriate amount of GO as crosslinker can strengthen the hydrogel, but the strengthening effect was weakened when the GO content was high. Meanwhile, the conductivity of the hydrogel with different GO contents was tested. As shown in Fig. 2b, the content of GO has no significant effect on the electrical conductivity (38.8–41.6 mS cm^{-1}) of the hydrogel. In the following study, the hydrogel with a 1 wt% GO content was used, unless otherwise stated.

In order to evaluate the rebounding resilience properties of hydrogels, a series of tensile loading and unloading cycles were applied to the hydrogels. As shown in Fig. 2c, the closed area of the stress–strain curve formed during the loading-unloading process increased with increasing the tensile strain, indicating that the dissipated energy also increased. This was due to the fact that the

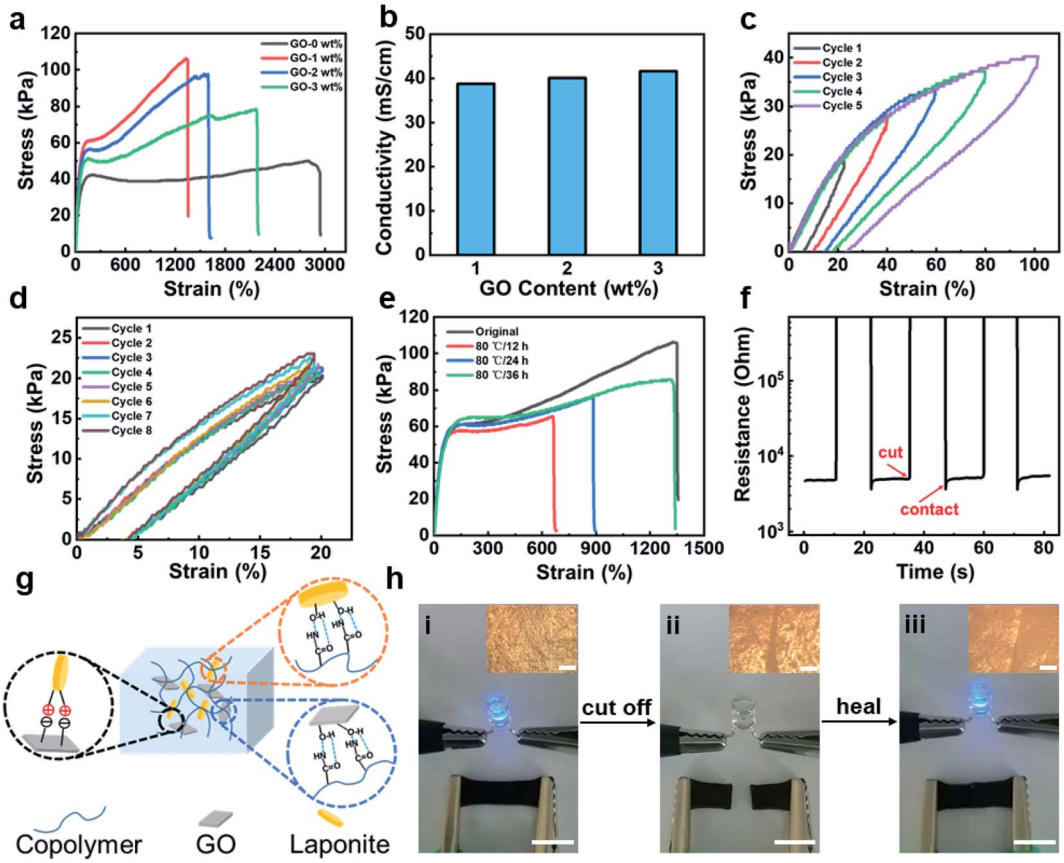

Fig. 2 Mechanical performance and healable property of the nanocomposite hydrogel. Tensile stress–strain curves (a) and ionic conductivity (b) of hydrogels with different contents of GO. Cyclic tensile behaviors of the hydrogel under different strains (c) and under a fixed strain without resting times (d). (e) Healable property of hydrogels healed at 80 °C for different time. (f) Time evolution of the healable process for the hydrogel by the real-time resistance measurements. (g) Schematic diagram of healable mechanism of hydrogels. (h) A circuit comprising hydrogel in series with a blue LED indicator: (i) original, (ii) completely bifurcated, (iii) healed. Inset: optical microscope image for the hydrogel at each state. Scale bar: 1 cm (i, ii, iii) and 200 μm (inset).

increase of strain leaded to the slip of more polymer chain segments and the dissipation of more energy.[37,38] Subsequently, we investigated the anti-fatigue properties of the hydrogel. As shown in Fig. 2d, in 8 consecutive cyclic tensile tests, the cycle curve of the hydrogel almost coincided with the initial state of the hydrogel, indicating that the hydrogel had good resilience and fatigue resistance. The thermal properties of hydrogels were studied by differential scanning calorimetry (DSC) experiments. The results show that dried hydrogels have a relatively high glass transition temperature (T_g) of 50.6–53.7 °C (Fig. S1†).

The healable properties of hydrogels were evaluated through the mechanical properties after cutting the hydrogel completely into two pieces and healing for different times. The healing efficiency calculated based on the strain to fracture is 50%, 60% and 99% after 12 h, 24 h and 36 h healing at 80 °C, respectively. Nevertheless, the healing efficiency is only 48% after 36 h healing at 25 °C (Fig. S2†). Besides, the healable properties of hydrogels were evaluated through the electrical properties. The time evolution of the resistance change is shown in Fig. 2f. When the hydrogel was completely cut off, the resistance increased sharply from the steady state to the open circuit state. Once the two broken samples were spliced together, the resistance value would quickly return to the initial value.

Fig. 2g showed a schematic diagram of the healable mechanism of the hydrogel. There were lots of oxygen-containing groups (–COOH, –OH, *etc.*) at the surface of GO.[39–41] There are also abundant –OH groups on the surface of Laponite plates; the surface of Laponite is negatively charged and the edge of Laponite is positively charged.[42] Therefore, both Laponite and GO can form hydrogen bondings with the $-CONH_2$ groups of the polymer chains and serve as the physical crosslinking points. These dynamic hydrogen bondings can then lead to the healable capability of the system, since they can be reversibly reformed after the damages. Furthermore, the reversible electrostatic interaction between the GO and the Laponite can also contribute to healable property of the hydrogel. For demonstration, the hydrogel was connected to the power source through the hydrogel and a commercial light-emitting diode (LED) bulb (Fig. 2h(i)). Hydrogel was cut into two pieces and attached back (Fig. 2h(ii) and 2h(iii)). The 67 μm wide cleft had almost disappeared, showing good repair ability (the inset photos in Fig. 2h). Moreover, there was no difference before and after the broken/healed process, thus verifying the healable of the electrical performance of the hydrogel. As for polymer ionic conductors, the ion conduction pathways are fully recovered as long as the molecular chains are healed; while for percolated polymer composites, the electron conduction pathways may not be thoroughly recovered after the healing process.

3.2 The output of TENG

The hydrogels and VHB elastomer are used as the electrodes and dielectric layer for TENGs. The TENG works in the single-electrode mode with a sandwich structure, in which hydrogel is used as an electrode, sealed between two layers of 3 M VHB membranes and connected to an external load with a copper wire. A commercial polytetrafluoroethylene (PTFE) film is used as the other electrification layer. Fig. 3a shows the working mechanism of TENG. When the PTFE surface is in contact with the VHB layer of the TENG, static charges of the same quantity and opposite polarity are generated on the PTFE and VHB surfaces, respectively (Fig. 3a–i). There is no potential difference between the two surfaces and no current is generated in the circuit. When the dielectric material PTFE is separated from the triboelectric layer VHB of the TENG, the un-screened positive static charges in VHB will induce the negative ions flowing to the gel/VHB interfaces. Thereby an electric double layer will be formed at the metal wire/gel interfaces, leading to the electrons flowing from the ground to the metal/gel interfaces through the

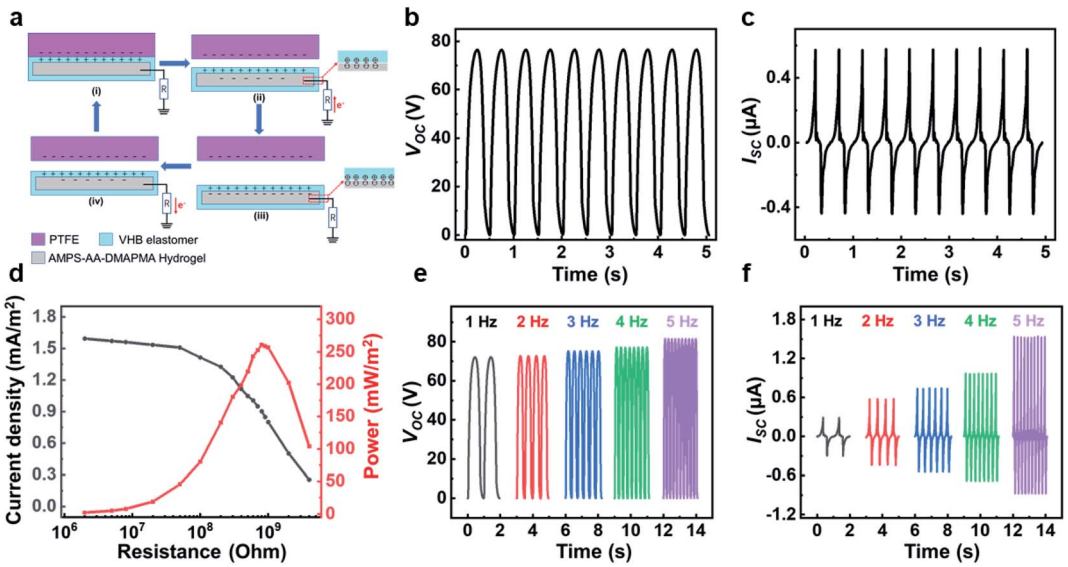

Fig. 3 The working principles and the output of the TENG with a single-electrode mode. (a) Scheme of the working mechanism of the TENG. The electric output performances of the TENG: (b) V_{oc}, (c) I_{sc}, and (d) Variation of the output current density and power density with the external loading resistance. (e) V_{oc} and (f) I_{sc} of the TENG under different driven frequency from 1 to 5 Hz.

external loading (Fig. 3a-ii). The electron stop flowing until all the static charges in the VHB are screened and the charge quantity of the electric double layer reaches maximum (Fig. 3b-iii). When PTFE is approaching by external force back to contact the TENG, the process is reversed, so that electrons will flow from the copper wire to the external circuit (Fig. 3b-iv). Alternating current will be generated when PTFE and TENG are engaged in continuous contact/separation movements.

The reciprocal contact-separation motion between a PTFE and a TENG (area, 2 × 2 cm^2) was realized by a linear motor. The motion frequency was firstly fixed to 2 Hz to measure the electrical output. As shown in Fig. 3b, c, and Fig. S3,† the open-circuit voltage (V_{oc}), short-circuit current (I_{sc}), and short-circuit charge (Q_{sc}) of TENGs are 75 V, 0.6 μA, and 25 nC, respectively. In addition, the output power density of the TENG was measured by changing the external resistance. When the external resistance is about 800 MOhm, the output power density of TENG reaches the maximum value of 260 mW m^{-2}. The TENG has obvious advantages over traditional electromagnetic generators in generating high-voltage electricity from irregular and low-frequency mechanical energies (<5 Hz).[43] By increasing the frequency, the Q_{sc} (Fig. S4†) and V_{oc} (Fig. 3e) showed very slight increase, as the generated static charge quantities are not sensitive to the motion frequency. Nevertheless, as the frequency increased from 1 Hz to 5 Hz, the I_{sc} increased from 0.3 μA to 1.5 μA (Fig. 3f). This is due to the fact that the time for charge transfer in each cycle is shortened at high frequency though the transferred charge quantity is about the same.

The actual application of TENG requires external mechanical stimulation or internal mechanical friction, which will inevitably damage TENG and directly affect the performance of TENG.[12,44] Therefore, it is necessary to develop TENG with healable property to recover its performances after damages. This hydrogel electrode has the healable capabilities, and the adhesive VHB film is also recoverable (Fig. S5†). It can be confirmed that the tensile strain of the VHB film can be recovered to be 55% after attaching the cut two pieces back into together in 1 min. We compared the output of TENG before and after healing process (Fig. 4 and Fig. S6†). There were no significantly changes in all three electrical output parameters (I_{sc}, V_{oc} and Q_{sc}), indicating that the hydrogel-based TENG could fully recover its output performances after damage.

The stretchability of the hydrogel-based TENG was evaluated at the stretched states (Fig. 4d–e and Fig. S7†). The output performances enhanced with the increase of strains. Compared with the initial state, the V_{oc}, I_{sc} and Q_{sc} reached ~164 V, ~1.6 μA and ~54 nC when increasing the strain to 500%. In the measurement process, the shape and size of PTFE film were larger than that of TENG at all stretched states. The increase in outputs is mainly caused by the change of contact surface area and dielectric layer thickness. The surface area of the TENG would increase under deformation conditions compared with the initial state, resulting in more static charges at a larger contact area. Meantime, the thickness of the VHB would decrease, which was also beneficial for the higher output. Similar results have also been reported.[30,31] Therefore, this TENG demonstrated exceptional ultra-stretchable performances. In addition, the durability of the device was also tested. As shown in Fig. 4f, TENG still showed stable performance after more than 3000 cycles under 2 Hz, indicating that the device had excellent long-term reliability.

3.3 TENG as power source for commercial electronics

TENG can usually be used as a sustainable nanoscale power source, harvesting tiny mechanical energy of human motion to power small electronics such as LED lights. The test was carried out by a TENG

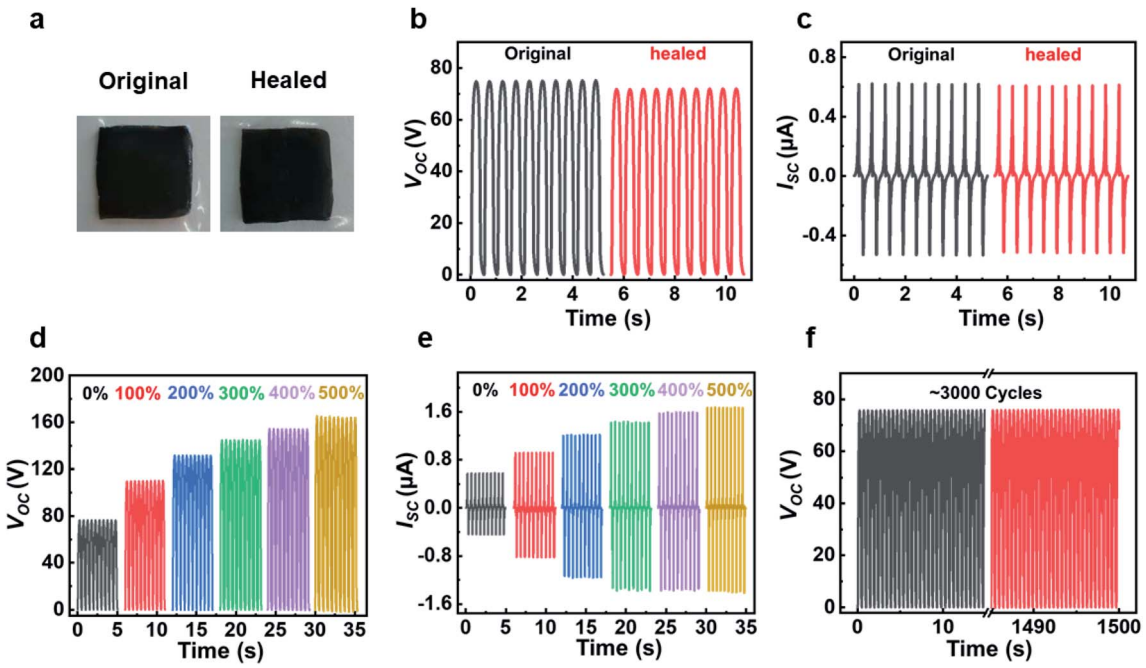

Fig. 4 The comparison of output for TENG before and after the healing process. (a) Photographs of the TENG before and healed after being cut in half. The comparison of the TENG output performances before and after healing. (b) V_{oc} and (c) I_{sc}. (d) V_{oc} and (e) I_{sc} of the TENG stretched to different strains. (f) The durability of the hydrogel-based TENG.

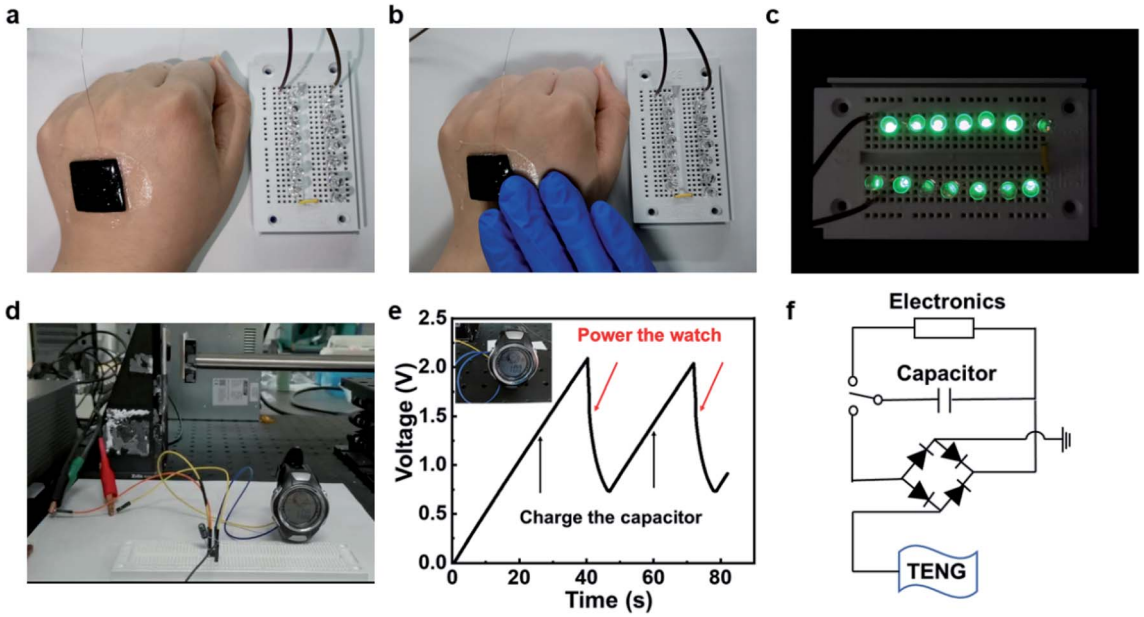

Fig. 5 Demonstration of the TENG to power commercial electronics. (a–c) Photograph of green LEDs connected in series driven by tapping the TENG with a hand. (d) An electric watch was powered by TENG. (e) Voltage profile of a 2.2 μF capacitor being charged by the TENG and powering the electronic watch. (f) The equivalent circuit of a self-charging system for the hydrogel based-TENG to power electronics.

with an area of 2 × 2 cm^2, and the human body can be regarded as a reference electrode or ground. As shown in Fig. 5a–c, 14 LED lights were successfully lit by tapping the TENG with a hand. Moreover, the TENG can be used to charge capacitors. Since TENG generates an AC signal, it cannot be used to power an electronic watch directly. A rectifier bridge is usually needed to manage the entire circuit. As shown in Fig. 5d and e, by connecting a rectifier, the generated electric energy can charge a 2.2 μF capacitor to 2 V within 40 s, and then power an electronic watch. The corresponding charging circuit diagram was shown in Fig. 5e.

3.4 Human motion detecting and pressure sensing by the TENG

The TENG could be utilized in various applications such as human motion monitoring and pressure sensing. As shown in

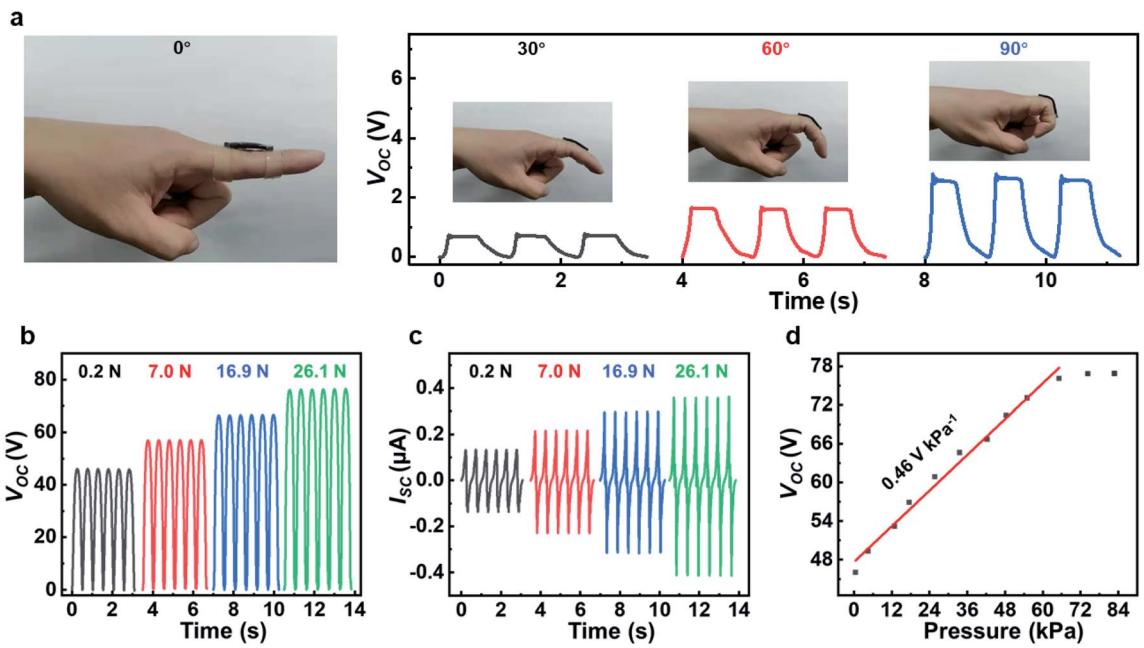

Fig. 6 TENG sensor for human motion detection and pressure sensing. (a) Open-circuit voltage responses when the TENG sensor has various bending angles on the finger joints. The V_{OC} (b) and I_{SC} (c) of the TENG as pressure sensor at different contact forces. (d) Summarized variation of peak amplitudes of the voltage with the contact pressure.

Fig. 6a, the TENG (30 mm × 5 mm) was designed and fixed on the finger to achieve contact separation movement when the finger was bent and straightened. When the bending angle of knuckles are periodically changed from 0° to 30–60–90°, the output V_{oc} of the TENG sensor increases from 0.7 V to 2.6 V correspondingly. When the bending angle increases, the contact area between the finger and the dielectric layer also increase, resulting in a corresponding enhance in the output of the TENG sensor. Several periodic repeatable outputs at each fixed angle demonstrate the dependability and repeatability of this self-powered wearable sensor. Moreover, TENG can also be used as self-powered sensors for force recognition. The output of TENG sensors were measured under a series of applied loading forces (Fig. 6b and c). Under higher pressure, higher output voltage and current can be observed. This is due to the fact that the micro-scale elastic deformation under high contact pressure leads to closer contact at the interface. So the effective contact area will increase, generating a higher electrical output. Fig. 6d shows the peak values of voltage output as a function of applied pressure. When the applied pressure is lower than 65 kPa, the peak value of V_{oc} increases at a rate of 0.46 V kPa^{-1}. When the pressure is higher than 65 kPa, the voltage values reach saturation.

4. Conclusion

In summary, we fabricated an ultra-stretchable and healable TENG, where VHB elastomer and ionic hydrogel were used as the electrification layer and electrode, respectively. The hydrogel exhibited high stretchability (~1356%) and high healable capability (~99% healing efficiency). The electricity generation capability of the TENG was demonstrated, which could be used as a sustainable self-powered power source to power commercial LED lights and electronic watches. The hydrogel-based TENG could also operate normally at 900% tensile strain and its electrical performances could be fully recovered after damages. In addition, this soft TNEG was demonstrated to be self-powered sensors for pressure sensing and human motion detection.

Conflicts of interest

The authors declare no conflict of interest.

Acknowledgements

The authors thank for the support from National Key Research and Development Program of China (2016YFA0202702), and the Youth Innovation Promotion Association of CAS and Youth Backbone Individual Project of Beijing Excellent Talents Training (Y9QNGG2701).

References

1 H. Park, Y. R. Jeong, J. Yun, S. Y. Hong, S. Jin, S. J. Lee, G. Zi and J. S. Ha, *ACS Nano*, 2015, **9**, 9974–9985.
2 M. Kaltenbrunner, T. Sekitani, J. Reeder, T. Yokota, K. Kuribara, T. Tokuhara, M. Drack, R. Schwodiauer, I. Graz, S. Bauer-Gogonea, S. Bauer and T. Someya, *Nature*, 2013, **499**, 458–463.
3 S. Zhao, J. Li, D. Cao, G. Zhang, J. Li, K. Li, Y. Yang, W. Wang, Y. Jin, R. Sun and C. P. Wong, *ACS Appl. Mater. Interfaces*, 2017, **9**, 12147–12164.
4 K. Tian, J. Bae, S. E. Bakarich, C. Yang, R. D. Gately, G. M. Spinks, M. In H. Panhuis, Z. Suo and J. J. Vlassak, *Adv. Mater.*, 2017, **29**, 1604827.
5 Y. Guo, S. Chen, L. Sun, L. Yang, L. Zhang, J. Lou and Z. You, *Adv. Funct. Mater.*, 2020, **20**, 2009799.
6 R. Hinchet, H. J. Yoon, H. Ryu, M. K. Kim, E. K. Choi, D. S. Kim and S. W. Kim, *Science*, 2019, **365**, 491–494.
7 Z. L. Wang, J. Chen and L. Lin, *Energy Environ. Sci.*, 2015, **8**, 2250–2282.
8 Y. Zi, S. Niu, J. Wang, Z. Wen, W. Tang and Z. L. Wang, *Nat. Commun.*, 2015, **6**, 8376.
9 Z. L. Wang, *ACS Nano*, 2013, **7**, 9533–9557.
10 C. Ye, Q. Xu, J. Ren and S. Ling, *Advanced Fiber Materials*, 2020, **2**, 24–33.
11 J. Kim, H. Ryu, J. H. Lee, U. Khan, S. S. Kwak, H. J. Yoon and S. W. Kim, *Adv. Energy Mater.*, 2020, **10**, 1903524.
12 J. Deng, X. Kuang, R. Liu, W. Ding, A. C. Wang, Y. C. Lai, K. Dong, Z. Wen, Y. Wang, L. Wang, H. J. Qi, T. Zhang and Z. L. Wang, *Adv. Mater.*, 2018, **30**, e1705918.
13 J. Sun, X. Pu, M. Liu, A. Yu, C. Du, J. Zhai, W. Hu and Z. L. Wang, *ACS Nano*, 2018, **12**, 6147–6155.
14 J. H. Lee, R. Hinchet, S. K. Kim, S. Kim and S.-W. Kim, *Energy Environ. Sci.*, 2015, **8**, 3605–3613.
15 Q. Guan, G. Lin, Y. Gong, J. Wang, W. Tan, D. Bao, Y. Liu, Z. You, X. Sun, Z. Wen and Y. Pan, *J. Mater. Chem. A*, 2019, **7**, 13948–13955.
16 J. Sun, W. Li, G. Liu, W. Li and M. Chen, *J. Phys. Chem. C*, 2015, **119**, 9061–9068.
17 H.-J. Kim, J.-H. Kim, K.-W. Jun, J.-H. Kim, W.-C. Seung, O. H. Kwon, J.-Y. Park, S.-W. Kim and I.-K. Oh, *Adv. Funct. Mater.*, 2016, **6**, 1502329.
18 Z. Wen, Y. Yang, N. Sun, G. Li, Y. Liu, C. Chen, J. Shi, L. Xie, H. Jiang, D. Bao, Q. Zhuo and X. Sun, *Adv. Funct. Mater.*, 2018, **28**, 1803684.
19 S. Chen, Y. Song, D. Ding, Z. Ling and F. Xu, *Adv. Funct. Mater.*, 2018, **28**, 1802547.
20 S. Kim, M. K. Gupta, K. Y. Lee, A. Sohn, T. Y. Kim, K. S. Shin, D. Kim, S. K. Kim, K. H. Lee, H. J. Shin, D. W. Kim and S. W. Kim, *Adv. Mater.*, 2014, **26**, 3918–3925.
21 U. Khan, T. H. Kim, H. Ryu, W. Seung and S. W. Kim, *Adv. Mater.*, 2017, **29**, 1603544.
22 K. Y. Chun, Y. Oh, J. Rho, J. H. Ahn, Y. J. Kim, H. R. Choi and S. Baik, *Nat. Nanotechnol.*, 2010, **5**, 853–857.
23 X. Chen, K. Parida, J. Wang, J. Xiong, M. F. Lin, J. Shao and P. S. Lee, *ACS Appl. Mater. Interfaces*, 2017, **9**, 42200–42209.
24 G.-H. Lim, S. S. Kwak, N. Kwon, T. Kim, H. Kim, S. M. Kim, S.-W. Kim and B. Lim, *Nano Energy*, 2017, **42**, 300–306.
25 H. Chen, Y. Xu, L. Bai, Y. Jiang, J. Zhang, C. Zhao, T. Li, H. Yu, G. Song, N. Zhang and Q. Gan, *Adv. Mater. Technol.*, 2017, **2**, 1700044.
26 S. Park, G. Thangavel, K. Parida, S. Li and P. S. Lee, *Adv. Mater.*, 2019, **31**, e1805536.

27 R. C. Chiechi, E. A. Weiss, M. D. Dickey and G. M. Whitesides, *Angew. Chem., Int. Ed. Engl.*, 2008, **47**, 142–144.
28 Y. Yang, N. Sun, Z. Wen, P. Cheng, H. Zheng, H. Shao, Y. Xia, C. Chen, H. Lan, X. Xie, C. Zhou, J. Zhong, X. Sun and S. T. Lee, *ACS Nano*, 2018, **12**, 2027–2034.
29 F. Yi, X. Wang, S. Niu, S. Li, Y. Yin, K. Dai, G. Zhang, L. Lin, Z. Wen, H. Guo, J. Wang, M. H. Yeh, Y. Zi, Q. Liao, Z. You, Y. Zhang and Z. L. Wang, *Sci. Adv.*, 2016, **2**, e1501624.
30 X. Pu, M. Liu, X. Chen, J. Sun, C. Du, Y. Zhang, J. Zhai, W. Hu and Z. L. Wang, *Sci. Adv.*, 2017, **3**, e1700015.
31 P. Zhang, Y. Chen, Z. H. Guo, W. Guo, X. Pu and Z. L. Wang, *Adv. Funct. Mater.*, 2020, **30**, 1909252.
32 J. P. Gong, *Science*, 2014, **344**, 161–162.
33 J. Du, R. Wu, H. Liu, X. Nie, H. Li, S. Xu and J. Wang, *Polym. Compos.*, 2015, **36**, 538–544.
34 P. Chen, S. Xu, R. Wu, J. Wang, R. Gu and J. Du, *Appl. Clay Sci.*, 2013, **72**, 196–200.
35 E. Zhang, T. Wang, L. Zhao, W. Sun, X. Liu and Z. Tong, *ACS Appl. Mater. Interfaces*, 2014, **6**, 22855–22861.
36 H. Li, T. Lv, H. Sun, G. Qian, N. Li, Y. Yao and T. Chen, *Nat. Commun.*, 2019, **10**, 536.
37 Z. Qin, R. Niu, C. Tang, J. Xia, F. Ji, D. Dong, H. Zhang, S. Zhang, J. Li and F. Yao, *Macromol. Mater. Eng.*, 2018, **303**, 1700396.
38 Z. Qin, D. Dong, M. Yao, Q. Yu, X. Sun, Q. Guo, H. Zhang, F. Yao and J. Li, *ACS Appl. Mater. Interfaces*, 2019, **11**, 21184–21193.
39 S. Stankovich, D. A. Dikin, R. D. Piner, K. A. Kohlhaas, A. Kleinhammes, Y. Jia, Y. Wu, S. T. Nguyen and R. S. Ruoff, *Carbon*, 2007, **45**, 1558–1565.
40 J. Shen, B. Yan, T. Li, Y. Long, N. Li and M. Ye, *Composites, Part A*, 2012, **43**, 1476–1481.
41 Y. Huang, M. Zeng, J. Ren, J. Wang, L. Fan and Q. Xu, *Colloids Surf., A*, 2012, **401**, 97–106.
42 N. N. Herrera, J.-M. Letoffe, J.-L. Putaux, L. David and E. Bourgeat-Lami, *Langmuir*, 2004, **20**, 1564–1571.
43 Y. Zi, H. Guo, Z. Wen, M. H. Yeh, C. Hu and Z. L. Wang, *ACS Nano*, 2016, **10**, 4797–4805.
44 T. P. Huynh, P. Sonar and H. Haick, *Adv. Mater.*, 2017, **29**, 1604973.